Resonance energy transfer near higher-order exceptional points of non-Hermitian Hamiltonians

Andrey Novitsky [1,2,*], Fyodor Morozko,[1,3] Dongliang Gao [4], Lei Gao,[4,5] Alina Karabchevsky,[3] and Denis V. Novitsky [1,6]

[1]*Belarusian State University, Nezavisimosti Avenue 4, 220030 Minsk, Belarus*
[2]*ITMO University, Kronverksky Prospekt 49, 197101 St. Petersburg, Russia*
[3]*School of Electrical and Computer Engineering, Ben-Gurion University, Beer-Sheva 8410501, Israel*
[4]*School of Physical Science and Technology, Soochow University, Suzhou 215006, China*
[5]*Department of Photoelectric Science and Energy Engineering, Suzhou City University, Suzhou 215104, China*
[6]*B. I. Stepanov Institute of Physics, National Academy of Sciences of Belarus, Nezavisimosti Avenue 68, 220072 Minsk, Belarus*

Exceptional points (EPs) of both eigenvalue and eigenvector degeneracy offer remarkable properties of the non-Hermitian systems based on the Jordanian form of Hamiltonians at EPs. Here we propose the perturbation theory able to underpin the physics in the vicinity of the higher-order EPs. The perturbation theory unveils lifting of degeneracy and origin of the different phases merging at the EP. It allows us to analyze the photonic local density of states and resonance energy transfer, determining their spectral behaviors in a general form. Resonant energy transfer is investigated in analytical and numerical examples. We analytically find the resonance energy transfer rate near the third-order EP occurring in the system of three coupled cavities and reveal singularities caused by the interplay of the perturbation and frequency detuning from degenerate eigenfrequency. Numerical simulation of the coupled-resonator system reveals the vital role of a mirror for switching to the EP of the doubled order and corresponding enhancement of the resonance energy transfer rate. Our investigation sheds light on the behavior of nanophotonic systems in non-Hermitian environments.

I. INTRODUCTION

In modern physics, non-Hermiticity is everywhere. It enriches our knowledge with new techniques and methodologies provoking researchers for searching groundbreaking applications. From the historical viewpoint, non-Hermitian Hamiltonians with real eigenvalues were proposed to compete with Hermitian ones to describe the quantum mechanics [1]. From this perspective, it has been recently shown that non-Hermitian Hamiltonians and Hermitian Hamiltonians are tightly related with a generalized vielbein formalism [2], while a prospective way of designing non-Hermitian topological systems with real-valued spectra was proposed in Ref. [3]. The most intriguing non-Hermitian Hamiltonian obeys parity-time (PT) symmetry, i.e., it simultaneously commutes with parity-inversion and time-reversal symmetry operators [4]. It is inspiring that non-Hermitian Hamiltonians can be introduced beyond quantum mechanics, the most fruitful theoretical and experimental results being obtained in optics.

Optical Hamiltonians stem from similarity of the Schrödinger equation and either Maxwell's equations or coupled-mode theory equations. To realize the PT symmetry in a nonmagnetic system, the Maxwell equations establish the necessary condition $\varepsilon(\mathbf{r}) = \varepsilon^*(-\mathbf{r})$, where the asterisk * denotes a complex conjugate. The PT symmetry breaks at the exceptional point (EP) that degenerates both the eigenvalues

and eigenvectors of the Hamiltonian. The latter takes a Jordanian form at the EP. Remarkable physics of the non-Hermitian systems near EPs was celebrated by a number of review articles [5–9] and promising theoretical and application-oriented results including enhancement of sensitivity [10–13], topological effects under encircling EPs [14–17], and CPA (coherent perfect absorption)-lasing [18–23] to mention just a few examples.

The benefits of non-Hermitian physics are still insufficiently exploited in nanophotonics that studies light-matter interaction at the nanoscale. In a theoretical work [24], the enhancement of the dipole's spontaneous emission rate was justified using the Green's function near the second-order EP. The theory was fully confirmed by measuring photoluminescence from active perovskite colloidal nanocrystals at the EP formed by coalescence of bright and dark modes of the one-dimensional dielectric grating [25]. For efficient trapping of atoms in Zeeman sublevels, the spontaneous relaxation rate from the excited to the ground state should be decreased. PT-symmetric cavities are able to significantly reduce the relaxation rate, opening avenues for quantum-optics applications [26]. The spontaneous emission can be perfectly inhibited as demonstrated in an open system of PT-symmetric rectangular waveguide [27]. Generally, the outstanding behavior of non-Hermitian systems is caused by the peculiar spectral response at the EP. In the case of the second-order EP, the line shape is described by the squared Lorentzian being dramatically different from the case of normal resonance [28]. Then, the spontaneous-emission decay strongly increases at the EP of the open quantum system [29]. In the microring

*andreyvnovitsky@gmail.com

195410-1

resonator with chiral EPs, both enhancement and suppression of the spontaneous emission of a quantum emitter is attainable, as shown in Ref. [30]. Interestingly, the modal Purcell factor corresponding to the part of the spontaneous emission coupled to guided modes was shown to be insensitive to existence of the EP [31]. Explanation of this fact was assumed to be related with the nonresonant character of PT-symmetric waveguides.

Another well-known nanophotonic phenomenon is the resonance energy transfer (RET), which represents the quantum-electrodynamical process of energy release by the donor molecule as a virtual photon and subsequent absorption of this photon by the acceptor molecule [32]. The energy transfer can be described in dipolar approximation, since the dipole transitions are the most probable ones. In this case, the mechanism was underpinned by Förster, who related the rate of energy transfer with the overlap of emission and absorption spectra and the distance between molecules [33,34]. In this paper, the donor and acceptor molecules are assumed to be dipoles with dipole moments $\mathbf{d}_D = |\mathbf{d}_D|\mathbf{e}_D$ and $\mathbf{d}_A = |\mathbf{d}_A|\mathbf{e}_A$, respectively. According to the Förster mechanism, the energy transfer rate is expressed by means of the donor luminescence spectrum $\sigma_{em}(\omega)$ and the acceptor absorption spectrum $\sigma_{\mathrm{abs}}(\omega)$ as [35,36]

$$\gamma_{D-A} = \int_0^\infty \sigma_{em}(\omega)\sigma_{\mathrm{abs}}(\omega)T(\omega)d\omega, \qquad (1)$$

where the two-point spectral density

$$T(\omega) = \frac{2\pi}{\hbar^2}\left(\frac{\omega^2}{\varepsilon_0 c}\right)^2 |\mathbf{d}_A \cdot \hat{G}(\omega, \mathbf{r}_D, \mathbf{r}_A) \cdot \mathbf{d}_D|^2 \qquad (2)$$

depends on the intermolecular distance $|\mathbf{r}_D - \mathbf{r}_A|$ and accounts for the environment through the dyadic Green's function $\hat{G}(\omega, \mathbf{r}_D, \mathbf{r}_A)$. Here ε_0 is the vacuum permittivity, $\hbar$ is the reduced Planck's constant, and c is the speed of light in vacuum. Note that the two-point spectral density function $T(\omega)$ used to describe RET between different points in space resembles more well-known local density of states (LDOS) [37], which is applied at a single point. LDOS is widely used in nanophotonics to explain and predict such effects as the modification of spontaneous emission rate [38,39] and Raman scattering [40,41] in the structured environment.

Correct treatment of the RET should be done within non-relativistic quantum electrodynamics because the photons mediating donor and acceptor are described nonclassically using the second quantization technique. Although a semi-classical description is valid in particular situations, only quantum electrodynamics is able to cover both radiative (R^{-2} dependence, where R is the distance between molecules) and nonradiative (R^{-6} dependence) RET. In Ref. [42], it is noted that the RET behaves both quantum mechanically and classically if one considers a donor-acceptor couple of molecules alone. However, in real life, this couple interacts with the surroundings and quantum decoherence should be taken into account. Nanophotonic environment plays an important part for control of the energy transfer via, e.g., surface plasmons [43–45] and hyperbolic metamaterials [36]. Influence of the surroundings (decoherence) can be reduced due to the restriction of small volumes being described within the cavity

quantum electrodynamics. In this case, polaritons are able to assist in enhancement of the cavity RET in the strong coupling regime [46–48].

In this paper, we analyze the role of non-Hermitian environments in control of the RET. To this end, we develop a perturbation theory in the vicinity of an EP of the nth order (EP$_n$) and describe non-Hermitian phases therein. Knowing the Green's function near the EP, we demonstrate the spectral behaviors of the LDOS and RET. Finally, we show examples of the RET dependencies for the higher-order ($n > 2$) EPs.

II. NON-HERMITIAN SYSTEMS: BASIC DEFINITIONS

A. Eigenvalue problem

Consider a system described by a non-Hermitian Hamiltonian $\hat{H} \neq \hat{H}^\dagger$, where $\dagger$ stands for the Hermitian conjugate. In this section, we formulate the general theory for the dimensionless Hamiltonian $\hat{H}$, which can be transformed to the physically justified Hamiltonian with multiplication by a dimensional coefficient. Then, eigenvalues $\lambda^{(m)}$ and eigenvectors $|v^{(m)}\rangle$ of $\hat{H}$ are dimensionless, too, and satisfy the eigenvalue equation

$$\hat{H}|v^{(m)}\rangle = \lambda^{(m)}|v^{(m)}\rangle, \quad m = 0,\dots n-1. \qquad (3)$$

If a Hamiltonian is PT-symmetric, i.e., it commutes with the parity-time operator $\hat{P}\hat{T}$, then its eigenvalues are real in a PT-symmetric state.

We also define n left eigenvectors $\langle u^{(m)}|$ meeting equation $\langle u^{(m)}|\hat{H} = \lambda^{(m)}\langle u^{(m)}|$ as well as the orthogonality and normalization conditions $\langle u^{(k)}|v^{(m)}\rangle = \delta_{km}$, where δ_{km} is the Kronecker delta. It allows one to decompose the Hamiltonian over projectors $|v^{(m)}\rangle\langle u^{(m)}|$ as

$$\hat{H} = \sum_{m=0}^{n-1} \lambda_m |v^{(m)}\rangle\langle u^{(m)}|. \qquad (4)$$

The inner product $\langle u^{(k)}|v^{(m)}\rangle$ may represent the product of the row $\langle u^{(k)}|$ and column $|v^{(m)}\rangle$ vectors or integral of two functions in an abstract vector space, e.g., $\langle u^{(k)}|v^{(m)}\rangle = \int u^{(k)}(x)v^{(m)}(x)dx$. In the case of a Hermitian Hamiltonian $\hat{H} = \hat{H}^\dagger$, the bra and ket vectors are related as $\langle u^{(k)}| = (|v^{(k)}\rangle)^\dagger$.

B. Green's function

The Green's function G of the Hamiltonian is defined as a solution $|v\rangle = G|J\rangle$ of the inhomogeneous Schrödinger equation with a source term $|J\rangle$:

$$\hat{H}|v\rangle + |J\rangle = \lambda|v\rangle. \qquad (5)$$

Expanding over the right eigenvectors $|v\rangle = \sum_{j=0}^{n-1} A_j|v^{(j)}\rangle$, multiplying Eq. (5) by the left eigenvector $\langle u^{(m)}|$ and applying the orthonormality condition, we write the Green's function (resolvent) as the Mittag-Leffler expansion [49]:

$$G = \sum_{m=0}^{n-1} \frac{1}{\lambda - \lambda^{(m)}} \frac{|v^{(m)}\rangle\langle u^{(m)}|}{\langle u^{(m)}|v^{(m)}\rangle}. \qquad (6)$$

Being an abstract representation of the Green's function, Eq. (6) can take different specific forms. If we deal with a

set of n coupled-mode equations for mode amplitudes a_j with corresponding mode electric fields $\mathbf{e}_j$, then the eigenvalue is the dimensionless frequency, $\lambda^{(m)} = \omega_m$, while the eigenvector $|v^{(m)}\rangle = (a_1^{(m)}, \ldots, a_n^{(m)})^T$ (see Refs. [29,50]). Being written in the basis of mode electric fields $\mathbf{e}_j$, the eigenvector recasts as $|v^{(m)}\rangle \to \sum_j a_j^{(m)} \mathbf{e}_j(\mathbf{r}) \equiv \mathbf{E}_m(\mathbf{r})$. By analogy, the left eigenvector $\langle u^{(m)}| = (b_1^{(m)}, \ldots, b_n^{(m)})$ in the conjugate basis $\tilde{\mathbf{e}}_j = (\mathbf{e}_j)^T$ takes the form $\langle u^{(m)}| \to \sum_j b_j^{(m)} \tilde{\mathbf{e}}_j(\mathbf{r}) \equiv \tilde{\mathbf{E}}_m(\mathbf{r})$. Assuming normalization $\langle u^{(m)}|v^{(m)}\rangle \to (\mathbf{E}_m \cdot \tilde{\mathbf{E}}_m) = 1$, the dyadic Green's function Eq. (6) reads

$$\hat{G}(\omega, \mathbf{r}, \mathbf{r}') = \sum_m \frac{\mathbf{E}_m(\mathbf{r}) \otimes \tilde{\mathbf{E}}_m(\mathbf{r}')}{\omega - \omega_m}. \tag{7}$$

If one deals with the archetypal Helmholtz equation $\nabla \times (\nabla \times \mathbf{E}) = (\omega/c)^2 \varepsilon(\mathbf{r})\mathbf{E}$ as in Ref. [24], then the Hamiltonian and eigenvalues are correspondingly $\hat{H} = c^2 \varepsilon^{-1} \nabla \times (\nabla \times)$ and $\lambda^{(m)} = \omega_m^2$. The dyadic Green's function can then be written as

$$\hat{G}(\mathbf{r}, \mathbf{r}') = \sum_m \frac{\mathbf{E}_m(\mathbf{r}) \otimes \mathbf{E}_m(\mathbf{r}')}{\omega^2 - \omega_m^2}. \tag{8}$$

Here, $\mathbf{E}_m(\mathbf{r})$ is the eigenvector meeting the equation $\hat{H}\mathbf{E}_m(\mathbf{r}) = \omega_m^2 \mathbf{E}_m(\mathbf{r})$. Notice that the eigenvalues $\lambda^{(m)}$ are generally complex.

C. Hamiltonian at the EP

Assume that the non-Hermitian Hamiltonian $\hat{H}(p)$ and, hence, the values $\lambda^{(m)}(p)$, $|v^{(m)}(p)\rangle$, and $\langle u^{(m)}(p)|$ depend on a parameter (parameters) p. If eigenvalues $\lambda^{(m)}$ and eigenvectors $|v^{(m)}\rangle$ ($k = 0, \ldots, n-1$) coalesce at a point p_0, then p_0 is an EP$_n$. The n-dimensional Hamiltonian at the EP takes a particular Jordan form

$$\hat{H}(p_0) \equiv \hat{H}_0 = \lambda^{(0)} I_n + \hat{N}, \tag{9}$$

where $\lambda^{(0)} = \lambda^{(0)}(p_0) = \ldots = \lambda^{(n-1)}(p_0)$, I_n is the unit matrix $n \times n$, and $\hat{N}$ is the nilpotent matrix [51]. The powers of the nilpotent matrix $\hat{N}^k$ are nonzero for $k < n$, while $\hat{N}^n = 0$. Degeneracy of the eigenvectors does not allow one to introduce a set of basis vectors. There are a single right eigenvector $|v^{(0)}\rangle$ and a single left eigenvector $\langle u^{(0)}|$ orthogonal to each other, $\langle u^{(0)}|v^{(0)}\rangle = 1$. They satisfy the ordinary eigenvalue equations, $\hat{H}_0|v^{(0)}\rangle = \lambda^{(0)}|v^{(0)}\rangle$ or $\hat{N}|v^{(0)}\rangle = 0$ and $\langle u^{(0)}|\hat{H}_0 = \lambda^{(0)}\langle u^{(0)}|$ or $\langle u^{(0)}|\hat{N} = 0$. The ordinary eigenvector $|v^{(0)}\rangle$ can be supplemented with a non-orthogonal set of the so-called generalized eigenvectors defined according to the chain equations $(\hat{H}_0 - \lambda^{(0)}I_n)|v^{(m)}\rangle = |v^{(m-1)}\rangle$ or $\hat{N}|v^{(m)}\rangle = |v^{(m-1)}\rangle$, where $m = 1, \ldots, n-1$. Thus, the nilpotent matrix can be defined as

$$N = \sum_{j=0}^{n-2} |v^{(j)}\rangle\langle u^{(n-2-j)}|, \tag{10}$$

where $\langle u^{(n-2-j)}|v^{(k)}\rangle = \delta_{j,k-1}$ or $\langle u^{(j)}|v^{(k)}\rangle = \delta_{n-2-j,k-1}$. Chain equations $\langle u^{(j)}|N = \langle u^{(j-1)}|$ ($j = 1, \ldots, n-1$) for generalized left eigenvectors are also consistent with Eq. (10).

The power $k = 1, \ldots, n-1$ of the nilpotent matrix N can be readily calculated, so we arrive at

$$N^k = \sum_{j=0}^{n-1-k} |v^{(j)}\rangle\langle u^{(n-1-k-j)}| \tag{11}$$

or

$$N^{n-k} = \sum_{j=0}^{k-1} |v^{(j)}\rangle\langle u^{(k-1-j)}|. \tag{12}$$

From the latter equation, it follows that $N^{n-1} = |v^{(0)}\rangle\langle u^{(0)}|$ and $N^{n-2} = |v^{(0)}\rangle\langle u^{(1)}| + |v^{(1)}\rangle\langle u^{(0)}|$.

III. PERTURBATION THEORY NEAR EP$_n$

Perhaps the most interesting properties of the non-Hermitian systems are observed at or close to the EP. The perturbation theory should be helpful in description of tiny departures from the EP. If a small parameter $|\varepsilon| \ll 1$ characterizes a deviation from the EP$_n$, then the Hamiltonian can be presented as $\hat{H} = \hat{H}_0 + \varepsilon\hat{H}_1$. Further, we assume that H_0 is a Jordan matrix of dimension n up to a similarity transformation that generates n eigenvalues with the leading term $\varepsilon^{1/n}$ when perturbed by the $\varepsilon\hat{H}_1$ operator [52]. By substituting the perturbation series for eigenvalues $\lambda = \sum_{k=0}^{\infty} \varepsilon^{k/n}\lambda_k$ and eigenvectors $|v\rangle = \sum_{m=0}^{\infty} \varepsilon^{m/n}|w_m\rangle$ into the eigenvalue equation $\hat{H}|v\rangle = \lambda|v\rangle$, we have

$$(\hat{H}_0 + \varepsilon\hat{H}_1)\sum_{m=0}^{\infty} \varepsilon^{m/n}|w_m\rangle = \sum_{k=0}^{\infty} \varepsilon^{k/n}\lambda_k \sum_{m=0}^{\infty} \varepsilon^{m/n}|w_m\rangle. \tag{13}$$

In a similar manner, we can write the eigenvalue equation for the left eigenvectors represented by the expansion $\langle u| = \sum_{m=0}^{\infty} \varepsilon^{m/n}\langle y_m|$.

Properly changing the summation indices, we arrive at the same power of the perturbation parameter ε on both sides of the above equation as

$$\sum_{m=0}^{\infty} \varepsilon^{m/n}(\hat{H}_0|w_m\rangle + \hat{H}_1|w_{m-n}\rangle) = \sum_{m=0}^{\infty}\sum_{k=0}^{\infty} \varepsilon^{m/n}\lambda_k|w_{m-k}\rangle, \tag{14}$$

where we have supplemented the sum $\sum_{m=k}^{\infty}$ on the right-hand side with zeros due to $|w_{m-k<0}\rangle = 0$ to get the same sums $\sum_{m=0}^{\infty}$ on both sides. By equating the terms having the same power of perturbation parameter on the right and left sides, we arrive at the infinite set of equations

$$(\hat{H}_0 - \lambda^{(0)}I_n)|w_m\rangle + \hat{H}_1|w_{m-n}\rangle = \sum_{k=1}^{m} \lambda_k|w_{m-k}\rangle. \tag{15}$$

If $m = 0$, then we are left with $(\hat{H}_0 - \lambda^{(0)}I_n)|w_0\rangle = 0$, that is, $|w_0\rangle = |v^{(0)}\rangle$.

For $0 < m < n$, Eq. (15) reads

$$(\hat{H}_0 - \lambda^{(0)}I_n)|w_m\rangle = \sum_{k=1}^{m} \lambda_k|w_{m-k}\rangle. \tag{16}$$

To determine the perturbation vectors $|w_m\rangle$, we decompose them over the nonorthogonal set of generalized

eigenvectors as

$$|w_m\rangle = \sum_{\alpha=0}^{n-1} c_{m,\alpha} |v^{(\alpha)}\rangle. \qquad (17)$$

Introducing this decomposition into Eq. (16), we derive the coefficients $c_{m,\alpha}$ as follows:

$$c_{0,0} = 1, \quad c_{m,\alpha>m} = 0,$$

$$c_{m,\alpha\leqslant m} = \sum_{k_1,\ldots,k_\alpha=1}^{k_1+\ldots+k_\alpha=m} \lambda_{k_1} \ldots \lambda_{k_\alpha}. \qquad (18)$$

See Appendix A for details on the origin of these relationships.

The correction terms λ_k of the eigenvalues stem from the perturbation and can be found from Eq. (15) for $m \geqslant n$, when the perturbation operator $\hat{H}_1$ is nonvanishing. The leading-order correction λ_1 splits the degenerate eigenvalue $\lambda^{(0)}$ into n different eigenvalues as follows:

$$\lambda^{(k)} = \lambda^{(0)} + \varepsilon^{1/n}\lambda_1^{(k)} = \lambda^{(0)} + \varepsilon^{1/n}(\langle u^{(0)}|\hat{H}_1|v^{(0)}\rangle)^{1/n}e^{i2\pi k/n}, \qquad (19)$$

where $k = 0, \ldots, n-1$. Appendix B shows how the leading-order and higher-order corrections can be obtained.

The perturbation coefficients both for eigenvalues and eigenvectors will be used further for finding the Green's function in the leading order.

IV. NON-HERMITIAN PHASES

A departure from the EP at p_0 may occur due to either external perturbation (nanoparticle, molecule, etc.) or variation of system's parameter p (gain, loss, coupling strength, etc.). In the latter case, the perturbation Hamiltonian originates from the Taylor series expansion as $\varepsilon\hat{H}_1 = \varepsilon(d\hat{H}/dp)_{p=p_0}$, where $\varepsilon = p - p_0$. The EP separates two phases distinguished by sign of the perturbation parameter $\varepsilon = \pm|\varepsilon|$. Nonzero ε lifts the degeneracy and the eigenvalues in the leading order of the expansion are equal to

$$\lambda^{(k)} = \lambda^{(0)} + (\pm|\varepsilon|)^{1/n}\lambda_1^{(k)}, \quad k = 0, \ldots, n-1. \qquad (20)$$

In the phase A of the non-Hermitian system, $\varepsilon > 0$ and the eigenvalues are

$$\lambda_A^{(k)} = \lambda^{(0)} + |\varepsilon|^{1/n}(\langle u^{(0)}|\hat{H}_1|v^{(0)}\rangle)^{1/n}e^{i2\pi k/n}. \qquad (21)$$

In the phase B, $\varepsilon < 0$ and the eigenvalues can be presented in the form

$$\lambda_B^{(k)} = \lambda^{(0)} + |\varepsilon|^{1/n}(\langle u^{(0)}|\hat{H}_1|v^{(0)}\rangle)^{1/n}e^{i\pi(2k+1)/n}. \qquad (22)$$

Notice that the EP of the nth order ($n > 2$) does not correspond to the situation usually observed with the PT-symmetric Hamiltonian, because the eigenvalues in both A and B phases are not real. On the other hand, for $n = 2$, the eigenvalues $k = 0, 1$ in both phases equal

$$\lambda_A^{(k)} = \lambda^{(0)} + |\varepsilon|^{1/2}(\langle u^{(0)}|\hat{H}_1|v^{(0)}\rangle)^{1/2}e^{i\pi k},$$

$$\lambda_B^{(k)} = \lambda^{(0)} + i|\varepsilon|^{1/2}(\langle u^{(0)}|\hat{H}_1|v^{(0)}\rangle)^{1/2}e^{i\pi k}, \qquad (23)$$

so one can clearly distinguish the nature of both phases. Their properties generally depend on the symmetry of the perturbation operator. If the real value $\langle u^{(0)}|\hat{H}_1|v^{(0)}\rangle > 0$, then the eigenvalues in phase A are real and this phase is PT symmetric whereas phase B corresponds to the broken-PT-symmetric phase. If, on the contrary, $\langle u^{(0)}|\hat{H}_1|v^{(0)}\rangle < 0$, then phase B is PT symmetric and phase A is broken-PT symmetric.

V. GREEN's FUNCTION NEAR EP$_n$

In this section, we derive the Green's function up to the leading order corresponding to the leading order of the eigenvalue

$$\lambda^{(k)} = \lambda^{(0)} + \delta\lambda^{(k)}, \quad \delta\lambda^{(k)} = \varepsilon^{1/n}\lambda_1^{(k)} = \varepsilon^{1/n}\eta e^{i2\pi k/n} \qquad (24)$$

and eigenvectors

$$|v^{(k)}\rangle = |v^{(0)}\rangle + |\delta v^{(k)}\rangle, \quad \langle u^{(k)}| = \langle u^{(0)}| + \langle\delta u^{(k)}|,$$

$$|\delta v^{(k)}\rangle = \sum_{m=1}^{\infty} \varepsilon^{m/n}|w_m^{(k)}\rangle, \quad \langle\delta u^{(k)}| = \sum_{m=1}^{\infty} \varepsilon^{m/n}\langle y_m^{(k)}|, \qquad (25)$$

where $k = 0, \ldots, n-1$ and $\eta = (\langle u^{(0)}|\hat{H}_1|v^{(0)}\rangle)^{1/n}$. More terms in vectors $|\delta v\rangle$ and $\langle\delta u|$ are needed to keep the first nonvanishing correction in further calculations.

In our notation, the Green's function Eq. (6) reads

$$G = \sum_{k=0}^{n-1} \frac{1}{\lambda - \lambda^{(0)} - \delta\lambda^{(k)}} \frac{|v^{(0)}\rangle\langle u^{(0)}| + |\delta v^{(k)}\rangle\langle u^{(0)}| + |v^{(0)}\rangle\langle\delta u^{(k)}|}{\langle\delta u^{(k)}|v^{(0)}\rangle + \langle u^{(0)}|\delta v^{(k)}\rangle + \langle\delta u^{(k)}|\delta v^{(k)}\rangle}, \qquad (26)$$

where we use the orthogonality $\langle u^{(0)}|v^{(0)}\rangle = 0$ in the denominator. The other inner products in the denominator are calculated in Appendix C, resulting in the value $\varepsilon^{\frac{n-1}{n}}\lambda_1^{n-1}$. In the nominator, the leading order of $|\delta v^{(k)}\rangle$ is $\varepsilon^{1/n}|w_1^{(k)}\rangle = \varepsilon^{1/n}c_{1,1}^{(k)}|v^{(1)}\rangle = \varepsilon^{1/n}\lambda_1^{(k)}|v^{(1)}\rangle$ and similarly $\langle\delta u^{(k)}| = \varepsilon^{1/n}\lambda_1^{(k)}\langle u^{(1)}|$. The Green's function then can be represented as

$$G = \frac{S_1|v^{(0)}\rangle\langle u^{(0)}| + \varepsilon^{1/n}\eta S_2(|v^{(1)}\rangle\langle u^{(0)}| + |v^{(0)}\rangle\langle u^{(1)}|)}{n\varepsilon^{(n-1)/n}\eta^{n-1}},$$

$$S_1 = \sum_{k=0}^{n-1} \frac{1}{(\lambda - \lambda^{(0)})\exp(-i2\pi k/n) - \varepsilon^{1/n}\eta}, \quad S_2 = \sum_{k=0}^{n-1} \frac{\exp(i2\pi k/n)}{(\lambda - \lambda^{(0)})\exp(-i2\pi k/n) - \varepsilon^{1/n}\eta}. \qquad (27)$$

The sums S_1 and S_2 calculated in Appendix D are equal to

$$S_1 = \frac{nb^{n-1}}{(-1)^{n-1}a^n + b^n}, \quad S_2 = -\frac{nab^{n-2}}{(-1)^{n-1}a^n + b^n}, \quad (28)$$

where $a = \lambda - \lambda^{(0)}$ and $b = -\varepsilon^{1/n}\eta$. Substituting S_1 and S_2 into the Green's function, we obtain

$$G = \frac{|v^{(0)}\rangle\langle u^{(0)}| + (\lambda - \lambda^{(0)})(|v^{(1)}\rangle\langle u^{(0)}| + |v^{(0)}\rangle\langle u^{(1)}|)}{(\lambda - \lambda^{(0)})^n - \varepsilon\langle u^{(0)}|\hat{H}_1|v^{(0)}\rangle}. \quad (29)$$

The Green's function can be written separately in the phase A ($\varepsilon > 0$), in the phase B ($\varepsilon < 0$), and at the EP ($\varepsilon = 0$). In the latter case, the Green's function G_{EP} in the leading order equals

$$G_{EP} = \frac{|v^{(0)}\rangle\langle u^{(0)}| + (\lambda - \lambda^{(0)})(|v^{(1)}\rangle\langle u^{(0)}| + |v^{(0)}\rangle\langle u^{(1)}|)}{(\lambda - \lambda^{(0)})^n}. \quad (30)$$

Since $N^{n-1} = |v^{(0)}\rangle\langle u^{(0)}|$ and $N^{n-2} = |v^{(1)}\rangle\langle u^{(0)}| + |v^{(0)}\rangle\langle u^{(1)}|$, we conclude that the derived Green's function is compatible with that in Refs. [53,54]. This means that we can generalize the Green's function in the vicinity of the EP including higher orders of the eigenvalue expansion:

$$G = \frac{(\lambda - \lambda^{(0)})^{n-1}I_n + \ldots + (\lambda - \lambda^{(0)})N^{n-2} + N^{n-1}}{(\lambda - \lambda^{(0)})^n - \varepsilon\langle u^{(0)}|\hat{H}_1|v^{(0)}\rangle}. \quad (31)$$

Thus, the nominator is defined by the eigenvalues and generalized eigenvectors at the EP, while the perturbation (probe) resides in the denominator changing positions of the poles (eigenmodes) [55]. When the deviation $\lambda - \lambda^{(0)}$ is small, the lower orders of $(\lambda - \lambda^{(0)})^k$ in nominator should be kept and we arrive at Eq. (29).

If the eigenvalue is the dimensionless frequency, $\lambda = \omega$, then the dyadic Green's function near the EP_n in the limit $|\omega - \omega_0| \ll 1$ reads

$$\hat{G}(\omega, \mathbf{r}, \mathbf{r}') = \frac{1}{(\omega - \omega_0)^n - \varepsilon\langle u^{(0)}|\hat{H}_1|v^{(0)}\rangle}[\mathbf{E}_0(\mathbf{r}) \otimes \tilde{\mathbf{E}}_0(\mathbf{r}') + (\omega - \omega_0)(\mathbf{E}_1(\mathbf{r}) \otimes \tilde{\mathbf{E}}_0(\mathbf{r}') + \mathbf{E}_0(\mathbf{r}) \otimes \tilde{\mathbf{E}}_1(\mathbf{r}'))], \quad (32)$$

where $\mathbf{E}_0$ and $\mathbf{E}_1$ introduced as in Eq. (7) are the normalized electric fields corresponding to the eigenvalue and Jordan generalized eigenvector, respectively.

VI. LOCAL DENSITY OF STATES NEAR EP_n

In the Green's function Eq. (32), ω is a real-valued frequency. However, ω_0 as a solution of the eigenvalue problem is generally complex, therefore, $\omega_0 = \omega_0' + i\omega_0''$, where the imaginary part ω'' accounts for both radiative and nonradiative relaxation rates of the eigenmode. Further, we adopt $|\omega_0''| \ll \omega_0'$.

The partial LDOS is defined as [35]

$$\rho(\omega) = \frac{6\omega}{\pi c^2}\text{Im}[\mathbf{e}_d \cdot \hat{G}(\omega, \mathbf{r}_d, \mathbf{r}_d) \cdot \mathbf{e}_d], \quad (33)$$

where $\mathbf{e}_d$ is a unit vector of dipole's orientation and $\mathbf{r}_d$ is the radius vector of dipole's position. The LDOS in an environ-
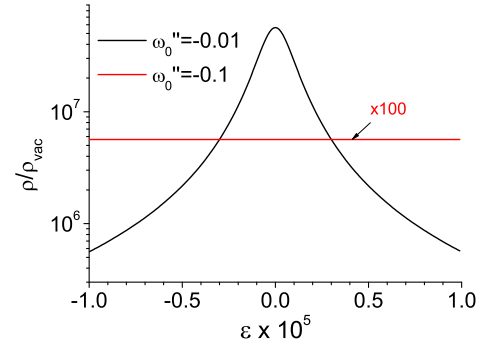

FIG. 1. Normalized. LDOS ρ/ρ_{vac} at the exceptional point of the third order versus perturbation parameter ε for different loss parameter ω_0''. Parameters: $\omega_0' = 1$, $\alpha = 1$, $\beta = 0$, and $\langle u_0|\hat{H}_1|v_0\rangle = 1$.

ment is usually scaled to the LDOS in vacuum defined as $\rho_{vac} = \omega^2/(\pi^2 c^3)$.

Substituting the Green's function Eq. (32) into the LDOS, we arrive at

$$\rho(\omega) = \frac{6\omega}{\pi c^2}\text{Im}\left(\frac{\alpha + \beta(\omega - \omega_0)}{(\omega - \omega_0)^n - \varepsilon\langle u^{(0)}|\hat{H}_1|v^{(0)}\rangle}\right), \quad (34)$$

where

$$\alpha = (\mathbf{e}_d \cdot \mathbf{E}_0(\mathbf{r}_d))(\tilde{\mathbf{E}}_0(\mathbf{r}_d) \cdot \mathbf{e}_d),$$

$$\beta = (\mathbf{e}_d \cdot \mathbf{E}_1(\mathbf{r}_d))(\tilde{\mathbf{E}}_0(\mathbf{r}_d) \cdot \mathbf{e}_d) + (\mathbf{e}_d \cdot \mathbf{E}_0(\mathbf{r}_d))(\tilde{\mathbf{E}}_1(\mathbf{r}_d) \cdot \mathbf{e}_d).$$

The LDOS at the EP (at $\varepsilon = 0$) can be analyzed in the closed form as given in Appendix E. To achieve the maximal LDOS, the denominator of the Green's function $(\omega - \omega_0)^n - \varepsilon\langle u^{(0)}|\hat{H}_1|v^{(0)}\rangle$ should be minimized. At the EP ($\varepsilon = 0$), the minimum corresponds to the frequency $\omega = \omega_0'$. Perturbation shifts this frequency off the value ω_0', but it still stays near ω_0'. The denominator of the LDOS depends on the loss ω_0'' and perturbation ε parameters. If ω_0'' is negligibly small, then the LDOS strongly depends on ε. This case is realized for a system of coupled high-Q cavities with low radiative losses [26,29]. In Fig. 1, which shows the LDOS near the third-order EP, the curve for $\omega_0'' = -0.01$ corresponds to strong enhancement of LDOS. On the contrary, when ω_0'' is relatively great, the effect of the perturbation $\varepsilon\langle u_0|\hat{H}_1|v_0\rangle$ is negligible and the LDOS does not change noticeably. This situation corresponds to open systems such as coupled waveguides [31]. In Fig. 1, the curve for $\omega_0'' = -0.1$ is $10^n = 10^3$ times wider and 10^3 times lower than the curve for $\omega_0'' = -0.01$. That is why it just looks like a horizontal line in the figure.

Parameters α and β exhibit the dependence on dipole's position $\mathbf{r}_d$. Dipole's position defines the extra phase of the electric field that can be accounted for by means of the complex parameter α, if $\beta = 0$. We observe in Fig. 2 how the complex number α influences symmetry of the LDOS function. If the order of the EP is even, then ρ is even (odd) function for imaginary (real) α in concordance with Eq. (E1) in Appendix E. When purely imaginary α flips signs, the LDOS function gets inverted. For the odd EP orders, the LDOS function is odd (even) for real (imaginary) α.

As we see in Fig. 2, the LDOS may take both positive and negative values. The negative LDOS is not physical and originates from the non-Hermitian nature of the Hamiltonian. In
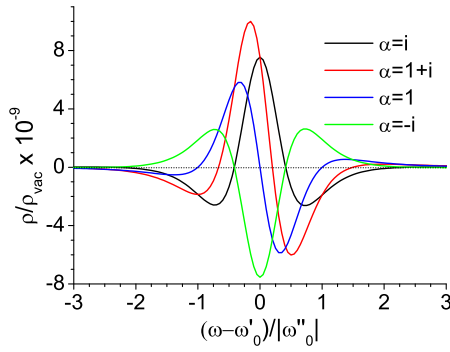
FIG. 2. Normalized LDOS ρ/ρ_{vac} at the EP of the fourth order versus frequency shift for different α. Parameters: $\omega_0' = 1$, $\omega_0'' = -0.01$, and $\beta = 0$.

this case, the classical definition of the LDOS is not applicable and we need to add an extra term related to dissipation and amplification given by the following formula [56]:

$$
\Delta\rho(\mathbf{r}_d, \omega)
$$
$$
= \frac{6\omega k^2}{\pi c^2} \int \mathrm{Im}[\varepsilon(\mathbf{r}', \omega)]|\mathbf{e}_d \cdot \hat{G}(\omega, \mathbf{r}_d, \mathbf{r}') \cdot \mathbf{e}_d|^2 d^3\mathbf{r}', \quad (35)
$$

where k is the wave number. Within our generic approach, we are not able to accurately take the non-Hermiticity into consideration because knowledge of gain and loss distributions and fields of the modes is needed. Albeit the LDOS in the paper is not fully correct without the term $\Delta\rho(\mathbf{r}_d, \omega)$, it well demonstrates the influence of non-Hermitian environments [57].

The EP order n strongly affects the height of the LDOS peak as demonstrated in Fig. 3. To guarantee a symmetric profile of the LDOS, we vary the values of parameter α. We see from Fig. 3 that the LDOS scales approximately as $A_n 10^{2n}$, where A_n is a constant. Thus, the spectral range in the vicinity of the EP_n can be used to reach an enormous increase in the LDOS and, therefore, the spontaneous decay rate defined according to Fermi's golden rule as $\gamma = (2\omega/3\hbar\varepsilon_0)|\mathbf{d}|^2\rho(\omega)$.
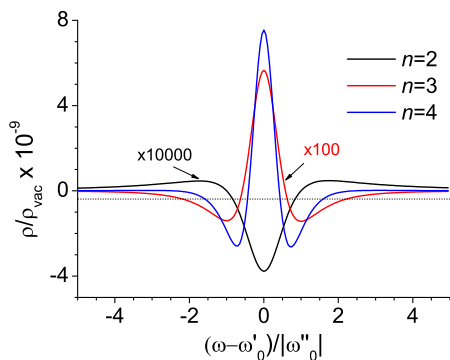

FIG. 3. Normalized LDOS ρ/ρ_{vac} at the EP versus frequency shift for different orders n of the EP. Parameters: $\omega_0' = 1$, $\omega_0'' = -0.01$, $\beta = 0$, and $\alpha = i$ for $n = 2, 4$ and $\alpha = 1$ for $n = 3$.
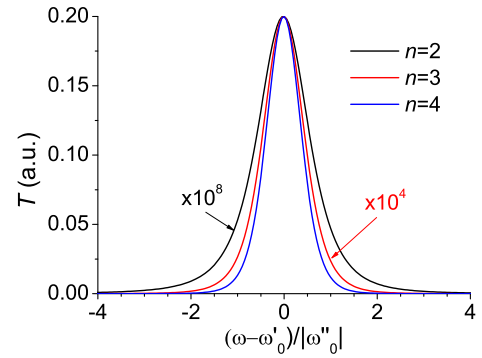

FIG. 4. The two-point spectral density $T(\omega)$ versus frequency shift for different orders n of the EP. Parameters: $\omega_0' = 1$, $\omega_0'' = -0.01$, and $A = B = 1 + i$.

VII. RET ENHANCEMENT NEAR EP_n

Modification of the resonant energy transfer rate due to the environment is described by the spectral density function $T(\omega)$ defined by Eq. (2) that depends on the two-point Green's function $\hat{G}(\omega, \mathbf{r}_A, \mathbf{r}_D)$ connecting the donor and acceptor dipoles. Near the EP, we obtain

$$
T(\omega) = \frac{2\pi}{\hbar^2} \left(\frac{\omega^2}{\varepsilon_0 c}\right)^2 \left| \frac{A + B(\omega - \omega_0)}{(\omega - \omega_0)^n - \varepsilon\langle u^{(0)}|\hat{H}_1|v^{(0)}\rangle} \right|^2, \quad (36)
$$

where

$$
A = (\mathbf{d}_A \cdot \mathbf{E}_0(\mathbf{r}_A))(\mathbf{E}_0(\mathbf{r}_D) \cdot \mathbf{d}_D),
$$
$$
B = (\mathbf{d}_A \cdot \mathbf{E}_1(\mathbf{r}_A))(\mathbf{E}_0(\mathbf{r}_D) \cdot \mathbf{d}_D) + (\mathbf{d}_A \cdot \mathbf{E}_0(\mathbf{r}_A))(\mathbf{E}_1(\mathbf{r}_D) \cdot \mathbf{d}_D).
$$

Under the approximation $\omega_0'' \ll \omega_0'$, the maximal spectral density T_{EP} at the EP ($\varepsilon = 0$) reads

$$
T_{EP}(\omega_0') = \frac{2\pi}{\hbar^2} \left(\frac{\omega_0'^2}{\varepsilon_0 c}\right)^2 \frac{|A|^2}{(\omega_0'')^{2n}}. \quad (37)
$$

Far from ω_0' ($|\omega - \omega_0'| \gg |\omega_0''|$), the quantity ω_0'' can be eliminated from the spectral density, resulting in

$$
T_{EP}(\omega) = \frac{2\pi}{\hbar^2} \left(\frac{\omega^2}{\varepsilon_0 c}\right)^2 \frac{|A + B(\omega - \omega_0')|^2}{(\omega - \omega_0')^{2n}}. \quad (38)
$$

As well as for the LDOS, the two-point spectral density demonstrated in Fig. 4 significantly increases at the EP. The enhancement of T is stronger than that of ρ, because the Green's function is squared in Eq. (36). However, in contrast to the LDOS, the spectral density $T(\omega)$ is always positive, providing us physically meaningful quantities. Being expressed by means of the Green's function, the LDOS and spectral density function cannot be simply related in the whole spectral range, but we can readily notice a direct proportionality of the maximal values of these quantities as $T(\omega_0') \sim \rho_{EP}^2(\omega_0')$.

The peak gets narrower when the order n increases. For finding the full width at half maximum $2\Delta\omega$, we can equate $T(\omega_0' + \Delta\omega) \approx \frac{2\pi}{\hbar^2}(\frac{(\omega_0')^2}{\varepsilon_0 c})^2 \frac{|A|^2}{\Delta\omega^{2n}}$ and $\frac{1}{2}T(\omega_0') = \frac{1}{2}\frac{2\pi}{\hbar^2}(\frac{(\omega_0')^2}{\varepsilon_0 c})^2 \frac{|A|^2}{(\omega_0'')^{2n}}$. It is clear that the peak width $2\Delta\omega$ decreases for higher EP orders n according to $2\Delta\omega = 2^{(2n+1)/2n}\omega_0''$. The width reduction is related to the increase

of the spectral function maximum $T(\omega')$ when the order n increases.

VIII. EP₃ IN THE SYSTEM OF COUPLED RESONATORS

Consider three coupled resonators, each of them having the same dimensionless eigenfrequency ω_0. Coupling coefficients are defined as follows: κ between resonators 1 and 2, $i\kappa$ between resonators 2 and 3, and $\alpha \exp(i\varphi)$ between 1 and 3. Then, the dimensionless non-Hermitian Hamiltonian reads

$$\hat{H}(\alpha) = \begin{pmatrix} \omega_0 & \kappa & \alpha e^{i\varphi} \\ \kappa & \omega_0 & i\kappa \\ \alpha e^{i\varphi} & i\kappa & \omega_0 \end{pmatrix}. \qquad (39)$$

The EP of the third order (EP₃) arises at $\alpha = 0$, when the eigenvalues of the Hamiltonian (Jordan matrix)

$$\hat{H}_0 = \hat{H}(0) = \begin{pmatrix} \omega_0 & \kappa & 0 \\ \kappa & \omega_0 & i\kappa \\ 0 & i\kappa & \omega_0 \end{pmatrix} \qquad (40)$$

are triply degenerate and equal to ω_0 (see Ref. [58]). The right eigenvector $|v^{(0)}\rangle = 2^{-1/2}(1, 0, i)^T$ follows from the eigenvalue equation $\hat{H}_0|v^{(0)}\rangle = \omega_0|v^{(0)}\rangle$. The left eigenvector $\langle u^{(0)}| = 2^{-1/2}(1, 0, i)$ can be determined in a similar way, from $\langle u^{(0)}|\hat{H}_0 = \omega_0\langle u^{(0)}|$. The normalization coefficient $2^{-1/2}$ is found from the condition $(|v^{(0)}\rangle)^\dagger |v^{(0)}\rangle = (\langle u^{(0)}|(\langle u^{(0)}|)^\dagger = 1$. As the eigenvalue theory of the Jordan matrices demands, the orthogonality condition $\langle u^{(0)}|v^{(0)}\rangle = 0$ is satisfied.

In the considered example, the perturbation parameter is the coupling strength, i.e., $\varepsilon = \alpha$, while the perturbation operator equals

$$\hat{H}_1 = \left.\frac{d\hat{H}(\alpha)}{d\alpha}\right|_{\alpha=0} = \begin{pmatrix} 0 & 0 & e^{i\varphi} \\ 0 & 0 & 0 \\ e^{i\varphi} & 0 & 0 \end{pmatrix}. \qquad (41)$$

Calculating the matrix element

$$\langle u^{(0)}|\hat{H}_1|v^{(0)}\rangle = ie^{i\varphi}, \qquad (42)$$

we readily write the three eigenvalues in each of the non-Hermitian phases A and B as

$$\omega_A^{(k)} = \omega_0 + \varepsilon^{1/3}e^{i\varphi/3 + i\pi/6}e^{i2\pi k/3},$$
$$\omega_B^{(k)} = \omega_0 + \varepsilon^{1/3}e^{i\varphi/3 + i\pi/6}e^{i\pi(2k+1)/3}, \qquad (43)$$

where $k = 0, 1, 2$.

The real and imaginary parts of the eigenvalues Eq. (43) are depicted in Fig. 5. At EP₃, $\varepsilon = 0$, the three eigenvalues coalesce. Departure from the EP₃ completely lifts the degeneracy, bringing us either to phase A for $\varepsilon > 0$ or phase B for $\varepsilon < 0$. We take $\varphi = \pi/3$ in the figure. In phase A, the eigenmode $k = 2$ is lossy, whereas the other two modes $k = 0, 1$ are amplifying. In phase B, the eigenmodes $k = 1, 2$ are lossy and only the mode $k = 0$ is amplifying. Mode $k = 0$ ($k = 2$) is amplifying (decaying) in both phases.

The two-point spectral density T [see Eq. (36)] responsible for the RET rate enhancement in the non-Hermitian environment has the form

$$T(\omega, \varepsilon, \varphi) = \frac{2\pi}{\hbar^2}\left(\frac{\omega^2}{\varepsilon_0 c}\right)^2 \left|\frac{A + B(\omega - \omega_0)}{(\omega - \omega_0)^3 - i\varepsilon \exp(i\varphi)}\right|^2. \qquad (44)$$
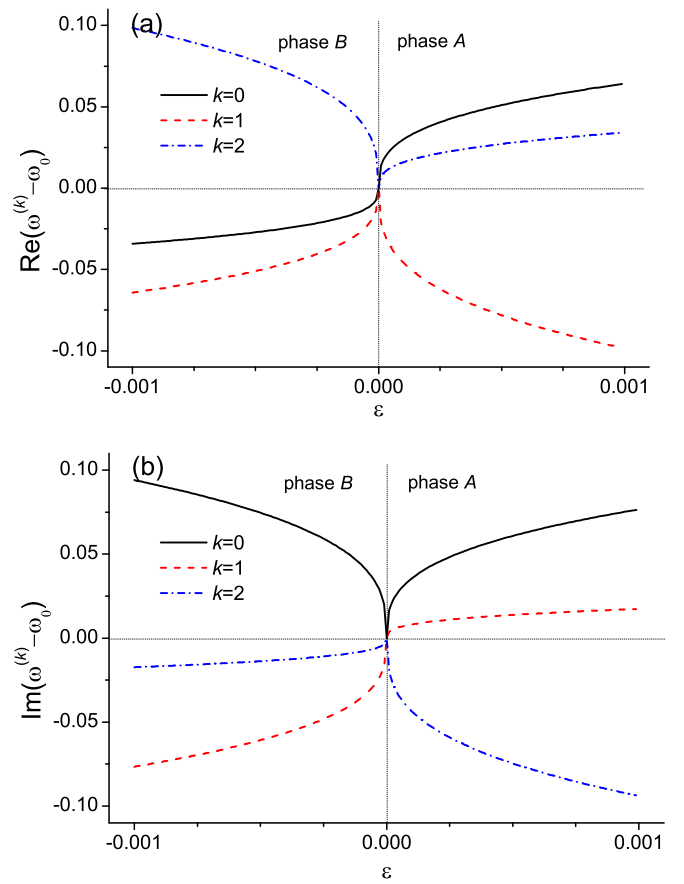

FIG. 5. (a) Real and (b) imaginary parts of eigenvalues $\omega^{(k)}$ according to Eq. (43) versus deviation ε from the EP₃ for $\varphi = \pi/3$.

In Fig. 6(a), we can see that the enhancement of the RET is not maximal at EP₃ ($\varepsilon = 0$). Deviation of the peak from the EP is caused by compensation of the perturbation ε and deviation from the eigenfrequency that minimizes the denominator in Eq. (44). To achieve a singularity of the spectral density, both the real and imaginary parts of the denominator should simultaneously vanish. This yields two equations,

$$\varepsilon \sin\varphi = -|\omega - \omega_0|^3 \cos(3\psi),$$
$$\varepsilon \cos\varphi = |\omega - \omega_0|^3 \sin(3\psi), \qquad (45)$$

where $\psi = \arctan[\omega_0''/(\omega_0' - \omega)]$. These equations are sufficient for writing coordinates of singular points in the parametric space (ε, φ) as follows:

$$\varepsilon = \pm|\omega - \omega_0|^3, \quad \varphi = \frac{\pi}{2} - 3\arctan\left(\frac{\omega_0''}{\omega_0' - \omega}\right) + \pi m, \qquad (46)$$

where m is integer. If $\omega = \omega_0'$ as in Fig. 6, then the singularities emerge at $\varepsilon = \omega_0''^3$, $\varphi = \pi$, and $\varepsilon = -\omega_0''^3$, $\varphi = 0$. Thus, despite the RET enhancement at the EP being finite, there are singular points of T in the neighborhood of the EP.

In Fig. 6(b), we observe different behaviors of the function T in the phase A (upper half-space) and B (lower half-space). In the phase A, we have a single singular point with the spectral peak corresponding to $\omega = \omega_0'$. When moving to the phase B, the single peak splits into two peaks with symmetrically located singularities. Positions of the singularities can
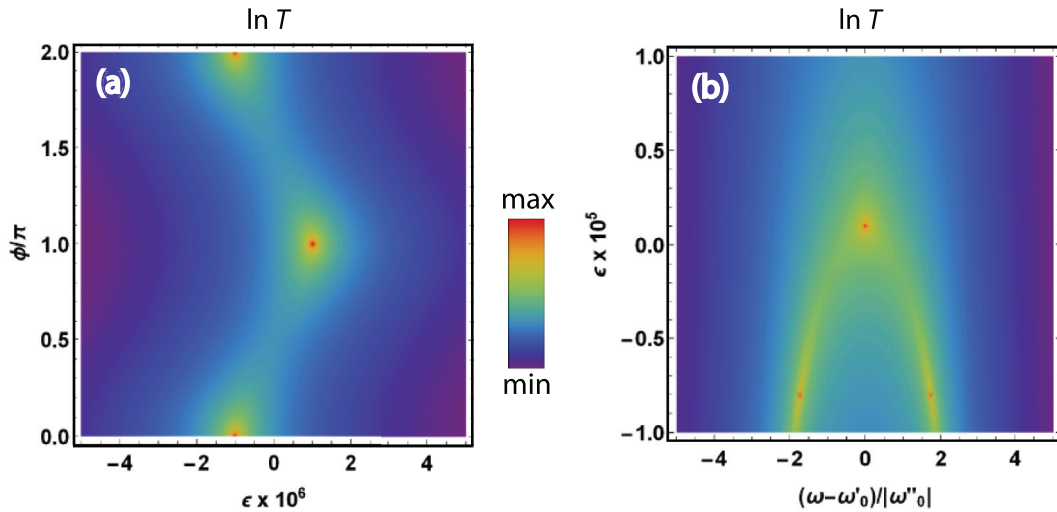
FIG. 6. The two-point spectral density $T(\omega, \varepsilon, \varphi)$ for EP$_3$ as a function of (a) the coupling parameter described by ε and φ at $\omega = 1$ and (b) ε and the frequency shift at $\varphi = \pi$. Parameters: $\omega_0' = 1$, $\omega_0'' = -0.01$, and $A = B = 1 + i$.

be determined using Eqs. (45). In the case shown in Fig. 6(b), $\varphi = \pi$ and, hence,

$$\varepsilon = -|\omega - \omega_0|^3 \sin(3\psi), \quad \cos(3\psi) = 0. \quad (47)$$

The solution of the latter equation is $3\psi = \pi/2 + \pi m$, where m is an integer number. Then, the frequency shift

$$\frac{\omega - \omega_0'}{-\omega_0''} = \cot\left(\frac{\pi}{6} + \frac{\pi m}{3}\right) \quad (48)$$

can be written for the three singularities as

$$\frac{\omega - \omega_0'}{-\omega_0''} = \begin{cases} \cot(\pi/6) = \sqrt{3}, & m = 0 \\ \cot(\pi/2) = 0, & m = 1 \\ -\cot(\pi/6) = -\sqrt{3}, & m = 2. \end{cases} \quad (49)$$

Taking the frequencies from this equation and substituting them into the first Eqs. (47), we get the perturbation parameters of the singular points as

$$\varepsilon = \begin{cases} -8|\omega''|^3, & m = 0 \\ |\omega''|^3, & m = 1 \\ -8|\omega''|^3, & m = 2. \end{cases} \quad (50)$$

These coordinates of the singular points obviously agree with those calculated in Fig. 6(b).

IX. RET IN THE SYSTEM OF NON-HERMITIAN MICRODISC RESONATORS

In a further example, we numerically study a system of two coupled microdisc resonators with attached waveguides as schematically shown in Fig. 7. The disks have the same radius equal to 5 μm, but their material parameters are different. The loss and gain microdiscs are characterized by the complex refractive indices $n_{\text{loss}} = n_r + in_i$ and $n_{\text{gain}} = n_r - in_i$, respectively, with $n_r = 2$ and $n_i = 2.539 \times 10^{-4}$. The waveguides coupled to the resonators are lossless and have the same refractive index n_r. The whole system is embedded into the background medium with the refractive index $n_0 = 1$. Distances between the discs and nearby waveguides 0.6 μm

are fixed, while the distance between the discs themselves is variable. Donor D and acceptor A molecules are modeled as electric dipoles. We place them in the gap between the discs.

In the non-Hermitian system described above, the eigenmodes of free-standing resonators are associated with complex eigenfrequencies $\omega_l = \omega_0' - i\gamma$ and $\omega_g = \omega_0' + i\gamma$. When the coupling coefficient κ between the resonators is equal to the loss-gain coefficient γ of the eigenmodes, a second-order EP emerges. If one attaches a mirror to one end of waveguide 1 (see Fig. 7), the system generally has a chiral exceptional hypersurface of order 2 for any value of coupling, except $\kappa = \gamma$, where it features an EP$_4$ (see Ref. [59] for details). Thus, one may reach an EP$_4$ in the system just using a mirror.

Without a mirror, each single resonator has two degenerate modes caused by the symmetry between clockwise (CW) and counter-clockwise (CCW) propagation directions. The mirror attached to waveguide 1 breaks this symmetry in the lossy microdisc, so only the CCW mode survives, as discussed in Ref. [60]. Interaction between these modes results in four supermodes ($k = 0, 1, 2, 3$) in the coupled system. Frequencies of supermodes are shown in Fig. 8 as a function of the distance between the discs d_{gap}. Figure 8(a) exhibits existence of EP$_2$ in
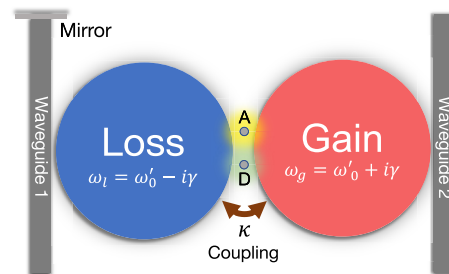

FIG. 7. A non-Hermitian system of coupled microdisc resonators to realize EP$_2$ and EP$_4$. Loss and gain resonators have respectively eigenfrequencies ω_l and ω_g. Coupling coefficient between discs equals κ.
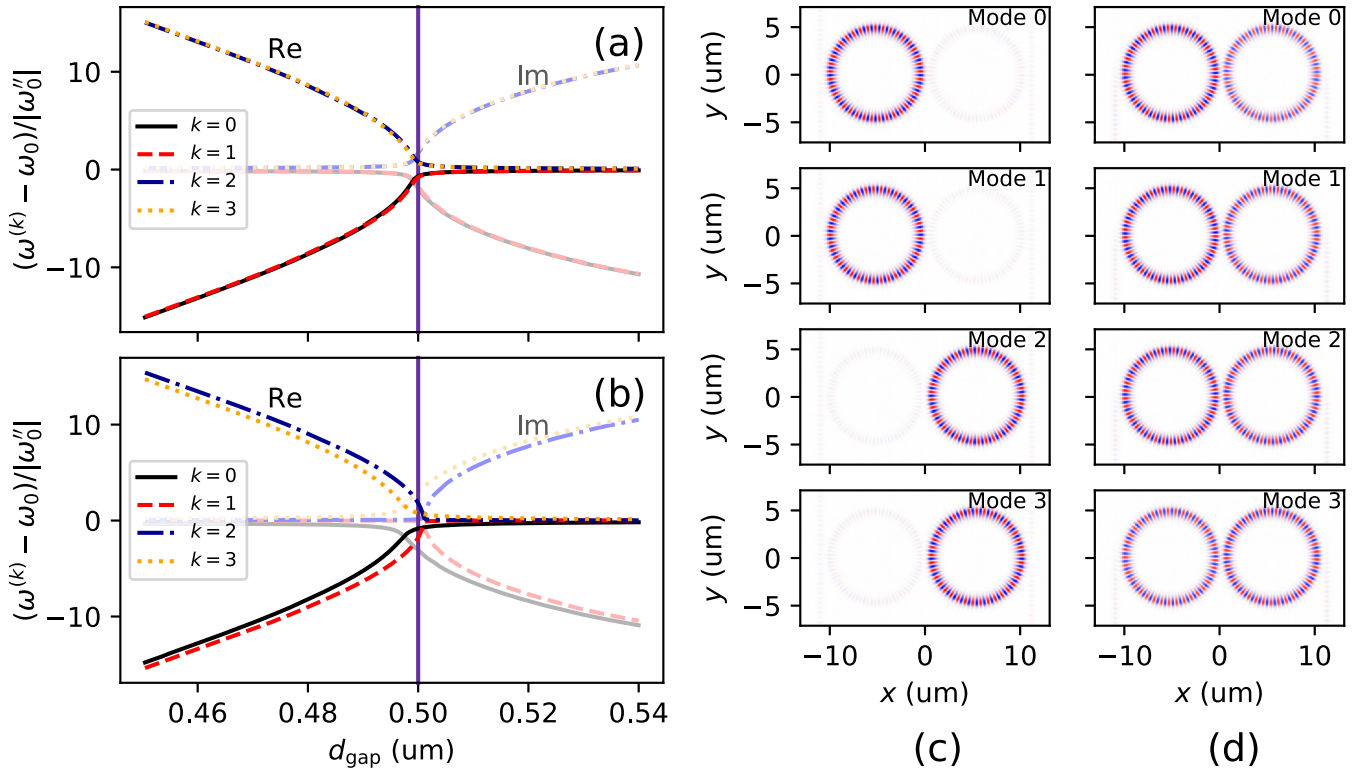
FIG. 8. (a), (b) Four complex eigenvalues of the system of coupled microdiscs (a) without and (b) with a mirror as a function of the distance between the disks $d_{\rm gap}$. Bright and dim curves correspond to the real and imaginary parts, respectively, in the same scale. (c), (d) Modal field profiles $\mathrm{Re}[f_k^z(\boldsymbol{r})]$ for supermodes of the system of coupled resonators (c) without a mirror (EP_2) and (d) with a mirror (EP_4). In (a)–(d), eigenfrequency $\omega_0 = (1266.7 - 9 \times 10^{-3}i)$ THz; in (c), (d) the distance between the disks is $d_{\rm gap} = 0.5\,\mu$m [it corresponds to a vertical line in (a) and (b)].

the system without the mirror near $d_{\rm gap} = d_0 = 500$ nm. Two couples of almost degenerate eigenvalues can also be observed in Fig. 8(b) for the design with the mirror. The structure of the eigenvectors in both cases, however, is different. In Fig. 8(a), the pairs of degenerate modes are linearly independent apart from $d_{\rm gap} = d_0$, thus forming two-dimensional subspaces. As seen in Fig. 8(c), the real parts of supermodes reside in different microdiscs while in Fig. 8(b) the modes coalesce, forming two exceptional hypersurfaces of the second order intersecting at d_0 to form EP_4. In this case, fields of the supermodes in Fig. 8(d) are distributed over the entire system and differ in phase.

To calculate the spectral density function $T(\omega)$, we utilize the coupled mode theory developed in Ref. [50] and find the quasinormal modes supported by the system. We expand the Green's function in terms of the single resonator modes $|\mathbf{f}_i\rangle$ as

$$G = \sum_{ik} B_{ik} |\mathbf{f}_i\rangle\langle\mathbf{f}_k|. \qquad (51)$$

The matrix of expansion coefficients B_{ik} stems from solving a matrix equation, which elements are defined by the overlap integrals. The Green's function has a diagonal form in the basis of supermodes as in Eq. (8), where ω_m and $\boldsymbol{E}_m$ are, respectively, complex eigenfrequencies and fields of the supermodes of the coupled microdisks. Expansion of the supermodes over the basis of single resonator modes is determined by means of diagonalization of the matrix B_{ik}.

Although the diagonalization of B_{ik} is needed for calculation of resonance frequencies in the coupled system, it is not necessary for calculating $T(\omega)$, as pointed out in Ref. [50]. Moreover, calculation in the basis of modes of bare resonators is advantageous owing to the fact that norms in this basis do not turn to zero at EPs, in contrast to those of the supermodes, which allows one to avoid Jordan expansion around the EP [50].

We calculate the E_z-polarized supermodes for the two-dimensional system of coupled resonators exploiting the procedure described in Ref, [50]. The quasinormal modes of single resonators are simulated using JCMsuite finite-element solver [61].

The spectral density $T(\omega)$ is calculated using Eq. (2) for the Green's function (51). $T(\omega)$ is demonstrated in Figs. 9 and 10 in the case of symmetric position of the donor and acceptor dipoles with respect to the microdiscs (see Fig. 7). As seen in Fig. 9, the presence of the mirror, making possible the EP_4, noticeably enhances the RET. Both mirror and mirror-free systems have a peak of the spectral density at the EP_2 characterized by $\omega \approx \omega_0'$ and $d_{\rm gap} \approx 500$ nm. The effect of the mirror is well demonstrated in Fig. 10. One notices sharpening of the resonance with an increase of the spectral density T when the mirror is present. Although the increase is not so pronounced as in the analytical dependencies in Fig. 4 since the numerical simulation is not fully optimized, one can notice narrowing of the resonance line shape as predicted by theory. One observes two types of curves in Fig. 10. At $d_{\rm gap} = 495$ nm,
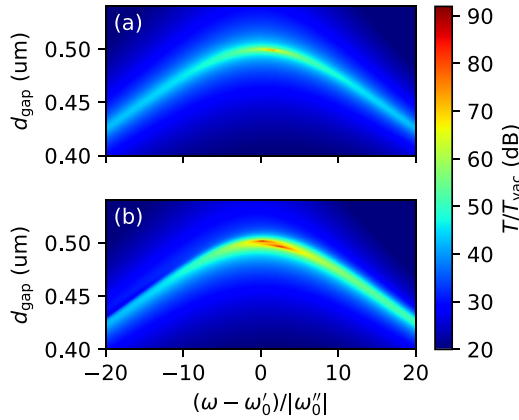
FIG. 9. Spectral density function $T(\omega)$ for two configurations, (a) without mirror and (b) with mirror, as a function of frequency and distance between the discs. Degenerate eigenfrequency equals $\omega_0 = 1266.7 - 9 \times 10^{-3}i$ THz. T_{vac} is the spectral density for the donor-acceptor pair in the free space [50].

there are two peaks at the frequencies on the left and on the right from $\omega = \omega_0'$. These peaks correspond to two couples of supermodes in the PT-symmetric phase. When increasing the interdisc distance d_{gap}, the peaks come closer and merge. On the other side from the EP, at $d_{\text{gap}} = 505$ nm, the single peak is associated with the broken PT-symmetric phase.

X. CONCLUSION

In this paper, we have developed a perturbation theory to determine the eigenvalues and eigenvectors near EPs of the nth order. Assuming that the leading order of the eigenvalue expansion is $\varepsilon^{1/n}$, we have proposed the algorithm for finding coefficients of the eigenvalue and eigenvector series. More intricate cases of the perturbation theory near EPs can be found in the literature [52,62,63]. The eigenvalues as a perturbation series have allowed distinguishing two phases in the non-Hermitian system corresponding to positive and negative values of the perturbation parameter. Using the perturbation theory, we have defined the Green's function near the EP of arbitrary order. This Green's function can be exploited for finding the LDOS and RET in non-Hermitian environments.
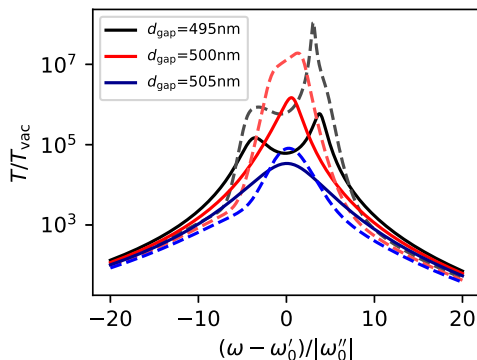

FIG. 10. Spectral density function $T(\omega)$ for several values of the parameter d_{gap}. Solid and dashed lines correspond to the resonators without and with the mirror, respectively.

The LDOS is shown to be either maximized or unaltered at the EP, if the losses of eigenmodes are small (for high-Q systems) or great (for low-Q systems), respectively. The similar behaviors can be found for RET. We have revealed the spectral dependencies of the LDOS and RET and demonstrated their features in several examples. In particular, we have considered a system of three coupled cavities possessing a third-order EP and determined the RET spectrum with singular points in each non-Hermitian phase. For a system of coupled microdiscs with attached waveguides, we consider a chiral non-Hermiticity induced by the mirror at the end of one of the waveguides. The mirror facilitate appearance of the EP of fourth order and, therefore, enhancement of the RET. We envisage benefits of our results in taking a deeper insight into nano-optics of non-Hermitian systems.

APPENDIX A: COEFFICIENTS $c_{m,\alpha}$

Equation (16) can be rewritten using the substitution $|w_m\rangle = \sum_{\alpha=0}^{m} c_{m,\alpha}|v^{(\alpha)}\rangle$ as

$$\sum_{\alpha=0}^{n-2} c_{m,\alpha+1}|v^{(\alpha)}\rangle = \sum_{k=1}^{m}\sum_{\alpha=0}^{n-1} c_{m-k,\alpha}\lambda_k|v^{(\alpha)}\rangle, \qquad \text{(A1)}$$

where we use the chain equation $(\hat{H} - \lambda^{(0)}I_n)|v^{(\alpha)}\rangle = |v^{(\alpha-1)}\rangle$ and change the summation index. Multiplying this equation by the left eigenvector $\langle u^{(\beta)}|$ and applying the orthonormalization conditions $\langle u^{(\beta)}|v^{(\alpha)}\rangle = \delta_{n-2-\beta,\alpha-1}$, we obtain the equation relating coefficients $c_{m,\alpha}$ to λ_k as

$$c_{m,\alpha+1} = \sum_{k=1}^{m} c_{m-k,\alpha}\lambda_k. \qquad \text{(A2)}$$

Since $|w_0\rangle = |v^{(0)}\rangle$ and simultaneously $|w_0\rangle = \sum_{\alpha=0}^{n-1} c_{0,\alpha}|v^{(\alpha)}\rangle$, we can write a kind of boundary condition for the coefficients $c_{m,\alpha}$ as follows: $c_{0,0} = 1$ and $c_{0,\alpha>0} = 0$. Using Eq. (A2), we readily get $c_{1,\alpha+1} = c_{0,\alpha}\lambda_1 = 0$ for $\alpha > 0$, which is equivalent to $c_{1,\alpha>1} = 0$. It is clear that, in general,

$$c_{m,\alpha>m} = 0. \qquad \text{(A3)}$$

This means that we have a set of orthogonality relations $\langle u^{(k)}|w_m\rangle = c_{m,n-1-k} = 0$, if $m < n - 1 - k$.

In a particular case of equal indices, the coefficients can be presented as $c_{m,m} = \sum_{k=1}^{m} c_{m-k,m-1}\lambda_k$. Since $c_{m-k,m-1} = 0$ for $k > 1$, there is a single nonzero term in the sum and $c_{m,m} = c_{m-1,m-1}\lambda_1$. Therefore,

$$c_{m,m} = c_{0,0}\lambda_1^m = \lambda_1^m. \qquad \text{(A4)}$$

Right eigenvector $|v^{(0)}\rangle$ can be excluded from the decomposition of vectors $|w_{m>0}\rangle$, because it has been already accounted for as a perturbation-free solution. This means that

the coefficients $c_{m,0} = \delta_{m,0}$, while

$$c_{m,1} = \sum_{k=1}^{m} c_{m-k,0} \lambda_k = \sum_{k=1}^{m} \delta_{m,k} \lambda_k = \lambda_m \qquad \text{(A5)}$$

and

$$c_{m,2} = \sum_{k=1}^{m} c_{m-k,1} \lambda_k = \sum_{k=1}^{m} \lambda_{m-k} \lambda_k. \qquad \text{(A6)}$$

In general, coefficients $c_{m,\alpha}$ are expressed in terms of λ_k as

$$c_{m,\alpha \leqslant m} = \sum_{\substack{k_1,\dots,k_\alpha=1}}^{k_1+\dots+k_\alpha=m} \lambda_{k_1} \dots \lambda_{k_\alpha}. \qquad \text{(A7)}$$

Thus, the perturbation vectors yield

$$|w_m\rangle = \sum_{\alpha=0}^{m} c_{m,\alpha}(\{\lambda_k\}) |v^{(\alpha)}\rangle. \qquad \text{(A8)}$$

Here m spans values from 0 to $n-1$ and $\{\lambda_k\}$ is the set of eigenvalue decomposition coefficients.

APPENDIX B: PERTURBATIVE CORRECTIONS λ_m TO EIGENVALUES

To determine λ_m, Eq. (15) at $m \geqslant n$ is multiplied by the left eigenvector $\langle u^{(0)}|$. Remembering that $\langle u^{(0)}|(\hat{H} - \lambda^{(0)} I_n) = 0$, we obtain

$$\langle u^{(0)}|\hat{H}_1|w_{m-n}\rangle = \sum_{k=1}^{m} \lambda_k \langle u^{(0)}|w_{m-k}\rangle. \qquad \text{(B1)}$$

Using the inner product $\langle u^{(k)}|w_m\rangle = c_{m,n-1-k}$ introduced in Appendix A, the right-hand side becomes $\sum_{k=1}^{m} \lambda_k c_{m-k,n-1}$ coinciding with the right-hand side of Eq. (A2). Thus, we write

$$c_{m,n \leqslant m} = \sum_{\alpha=0}^{m} c_{m-n,\alpha} \langle u^{(0)}|\hat{H}_1|v^{(\alpha)}\rangle. \qquad \text{(B2)}$$

For $m = n$, we know that $c_{n,n} = \lambda_1^n$ and $c_{0,\alpha} = \delta_{0,\alpha}$. Then the degeneracy is removed and the leading-order correction for eigenvalues $k = 0, \dots, n-1$ reads

$$\lambda_1^{(k)} = (\langle u^{(0)}|\hat{H}_1|v^{(0)}\rangle)^{1/n} e^{i2\pi k/n}. \qquad \text{(B3)}$$

Up to the end of this Appendix, the superscript (k) will be dropped, but we keep in mind that the expressions we derive correspond to a certain eigenvalue. The following perturbation term λ_2 can be found from

$$c_{n+1,n} = \sum_{\alpha=0}^{n+1} c_{1,\alpha} \langle u^{(0)}|\hat{H}_1|v^{(\alpha)}\rangle. \qquad \text{(B4)}$$

On the right-hand side of this equation, there is a single non-vanishing coefficient $c_{1,1} = \lambda_1$, while on the left-hand side, we have the sum of products of λ_1^{n-1} and λ_2 according to the relationship Eq. (A7):

$$n\lambda_1^{n-1} \lambda_2 = \lambda_1 \langle u^{(0)}|\hat{H}_1|v^{(1)}\rangle. \qquad \text{(B5)}$$

Thus, we get

$$\lambda_2 = \frac{1}{n} \lambda_1^{2-n} \langle u^{(0)}|\hat{H}_1|v^{(1)}\rangle. \qquad \text{(B6)}$$

Perturbation term λ_{p+1} can be taken from

$$\sum_{k_1,\dots,k_n=1}^{k_1+\dots+k_n=n+p} \lambda_{k_1} \dots \lambda_{k_n} = \sum_{\alpha=0}^{p} c_{p,\alpha} \langle u^{(0)}|\hat{H}_1|v^{(\alpha)}\rangle. \qquad \text{(B7)}$$

On the left-hand side of this equation, we can always distinguish the highest-order perturbation term λ_{p+1} (the remainder of this sum depending on $\lambda_1, \dots, \lambda_p$ is denoted Σ'), then

$$C_n^1 \lambda_1^{n-1} \lambda_{p+1} + \Sigma' = \sum_{\alpha=0}^{p} c_{p,\alpha} \langle u^{(0)}|\hat{H}_1|v^{(\alpha)}\rangle \qquad \text{(B8)}$$

and correction equals

$$\lambda_{p+1} = \frac{1}{n} \lambda_1^{1-n} \left[\sum_{\alpha=0}^{p} c_{p,\alpha} \langle u^{(0)}|\hat{H}_1|v^{(\alpha)}\rangle - \Sigma' \right]. \qquad \text{(B9)}$$

The remainder Σ' is the known quantity, because it depends on the lower-order corrections that can be found in a similar way.

APPENDIX C: DENOMINATOR OF THE GREEN'S FUNCTION Eq. (26)

Owing to the similarity of the perturbation theory for left $\langle u|$ and right $|v\rangle$ eigenvectors, the inner products $\langle \delta u^{(k)}|v^{(0)}\rangle$ and $\langle u^{(0)}|\delta v^{(k)}\rangle$ coincide, being equal to

$$\langle \delta u^{(k)}|v^{(0)}\rangle = \langle u^{(0)}|\delta v^{(k)}\rangle = \sum_{m=1}^{\infty} \varepsilon^{\frac{m}{n}} \langle u^{(0)}|w_m^{(k)}\rangle$$

$$= \sum_{m=1}^{\infty} \varepsilon^{\frac{m}{n}} c_{m,n-1} \approx \varepsilon^{\frac{n-1}{n}} c_{n-1,n-1} = \varepsilon^{\frac{n-1}{n}} \lambda_1^{n-1} \qquad \text{(C1)}$$

in the leading order, where we use the expansion for $|w_m^{(k)}\rangle$ and equality $c_{m,\alpha>m} = 0$. One more term in the denominator of the Green's function Eq. (26) can be written as

$$\langle \delta u^{(k)}|\delta v^{(k)}\rangle = \sum_{m=1}^{\infty} \sum_{m'=1}^{\infty} \varepsilon^{\frac{m+m'}{n}} \langle y_m^{(k)}|w_{m'}^{(k)}\rangle. \qquad \text{(C2)}$$

In the decomposition $\langle y_m| = \sum_{\alpha=0}^{n-1} d_{m,\alpha} \langle u^{(\alpha)}|$, similar to that for $|w_m\rangle$, the coefficients $d_{m,\alpha}$ meet the same relationships as $c_{m,\alpha}$. The inner product can be presented as

$$\langle y_m|w_{m'}\rangle = \sum_{\alpha,\alpha'} d_{m,\alpha} c_{m',\alpha'} \langle u^{(\alpha)}|v^{(\alpha')}\rangle = \sum_{\alpha=0}^{n-1} d_{m,\alpha} c_{m',n-1-\alpha}, \qquad \text{(C3)}$$

where we account for the orthonormalization condition $\langle u^{(\alpha)}|v^{(\alpha')}\rangle = \delta_{n-2-\alpha,\alpha'-1}$. As we have discussed earlier, nonzero coefficients d and c are realized for, respectively, $\alpha \leqslant m$ and $n-1-\alpha \leqslant m'$, that is, for $m + m' \geqslant n-1$. In the leading order, $m + m'$ should be minimal and, hence, takes the value $n-1$. Then the single term corresponding to $m' = n-1-m$ is left in the sum over m':

$$\langle \delta u^{(k)}|\delta v^{(k)}\rangle = \sum_{m=1}^{n-2} \varepsilon^{\frac{n-1}{n}} \langle y_m^{(k)}|w_{n-1-m}^{(k)}\rangle. \qquad \text{(C4)}$$

A couple of inequalities $\alpha \leqslant m$ and $n-1-\alpha \leqslant m'$ in the case $m' = n-1-m$ recasts as $\alpha \leqslant m$ and $\alpha \geqslant m$, bringing

us also to the single value $\alpha = m$. Then the inner product is reduced to

$$\langle y_m | w_{n-1-m} \rangle = c_{n-1-m,n-1-m} d_{m,m} = \lambda_1^{n-1-m} \lambda_1^m = \lambda_1^{n-1}. \tag{C5}$$

It does not depend on m, therefore, we rewrite Eq. (C4) as

$$\langle \delta u^{(k)} | \delta v^{(k)} \rangle = \varepsilon^{\frac{n-1}{n}} (n-2) \lambda_1^{n-1}. \tag{C6}$$

The denominator of the Green's function Eq. (26) in the leading order, thus, equals $\varepsilon^{\frac{n-1}{n}} \lambda_1^{n-1}$.

APPENDIX D: CALCULATION OF SUMS S_1 AND S_2

Closed-form expressions for the sums over eigenmodes can be determined using the auxiliary function $F(a,b)$ defined as a common denominator of S_1 and S_2:

$$F(a,b) = \prod_{k=0}^{n-1} [a \exp(-i2\pi k/n) + b], \tag{D1}$$

where $a = \lambda - \lambda^{(0)}$ and $b = -\varepsilon^{1/n} \eta$. The function F can be straightforwardly calculated; it equals

$$F(a,b) = (-1)^{n-1} a^n + b^n. \tag{D2}$$

At the same time, the sums can be written in terms of the derivatives and indefinite integral as follows:

$$S_1 = \frac{1}{F} \frac{\partial F}{\partial b}, \quad S_2 = \frac{\partial}{\partial b} \int S_1 da. \tag{D3}$$

After some algebra, we arrive at Eqs. (28).

APPENDIX E: LDOS AT THE EP

Here we study the LDOS given by Eq. (34) at $\varepsilon = 0$. In general, the field parameters $\alpha = \alpha' + i\alpha''$ and $\beta = \beta' + i\beta''$ are complex. Then the LDOS takes the form

$$\rho_{\mathrm{EP}}(\omega) = \frac{6\omega[n\tilde{\alpha}'\omega_0'' + \tilde{\alpha}''\Delta\omega + (n-1)\tilde{\beta}'\omega_0''\Delta\omega + \tilde{\beta}''\Delta\omega^2]}{\pi c^2 \Delta\omega^{n+1}}, \tag{E1}$$

where $\Delta\omega = ((\omega - \omega_0')^2 + \omega_0''^2)^{1/2}$, $\tilde{\alpha}' = \alpha'[\mathrm{sgn}(\omega - \omega_0')]^{n-1}$, $\tilde{\alpha}'' = \alpha''[\mathrm{sgn}(\omega - \omega_0')]^n$, $\tilde{\beta}' = \beta'[\mathrm{sgn}(\omega - \omega_0')]^{n-2}$, and $\tilde{\beta}'' = \beta''[\mathrm{sgn}(\omega - \omega_0')]^{n-1}$.

Assume first that real and imaginary parts of α and β are nonzero and much greater than ω_0''. The LDOS is maximized at the frequency $\omega = \omega_0'$ corresponding to the minimal denominator. In this case, $\Delta\omega = \omega_0''$ and the LDOS at the EP is great, but finite:

$$\rho_{\mathrm{EP}}(\omega_0') = \frac{6\omega_0'[n\tilde{\alpha}' + \tilde{\alpha}'']}{\pi c^2 (\omega_0'')^n}. \tag{E2}$$

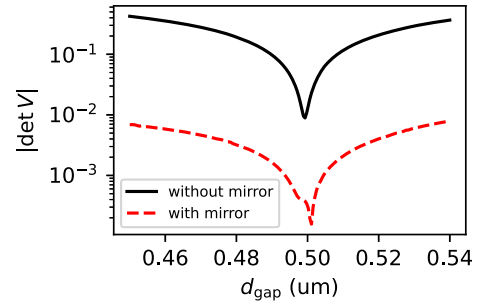Here we have neglected the terms proportional to ω_0'' in the nominator.

FIG. 11. Determinant of the eigenvector matrix V.

In the limit $|\omega - \omega_0'| \gg |\omega_0''|$, the terms containing ω_0'' can be neglected, resulting in

$$\rho_{\mathrm{EP}}(\omega) = \frac{6\omega[\alpha'' + \beta''(\omega - \omega_0')]}{\pi c^2 (\omega - \omega_0')^n}. \tag{E3}$$

If dipole's polarization is orthogonal to mode's polarization, so either $(\mathbf{e}_d \cdot \mathbf{E}_0(\mathbf{r})) = 0$ or $(\tilde{\mathbf{E}}_0(\mathbf{r}) \cdot \mathbf{e}_d) = 0$, then $\alpha = 0$ and we get

$$\rho_{\mathrm{EP}}(\omega) = \frac{6\omega[(n-1)\tilde{\beta}'\omega_0'' + \tilde{\beta}''\Delta\omega]}{\pi c^2 \Delta\omega^n}. \tag{E4}$$

Then, at $\omega = \omega_0'$, the peak is less pronounced, being

$$\rho_{\mathrm{EP}}(\omega_0') = \frac{6\omega_0'[(n-1)\tilde{\beta}' + \tilde{\beta}'']}{\pi c^2 (\omega_0'')^{n-1}}. \tag{E5}$$

APPENDIX F: MODES OF NON-HERMITIAN COUPLED MICRODISKS

Hybrid quasinormal modes of the coupled system are expanded over basis modes as

$$|\tilde{\mathbf{f}}_k\rangle = \sum_i V_{ik} |\mathbf{f}_i\rangle, \tag{F1}$$

where V_{ik} is a 4×4 matrix of expansion coefficients, each column of which is a vector of a hybrid mode in the basis $|\mathbf{f}_i\rangle$. These columns are also the eigenvectors of the Hamiltonian matrix. At an EP, two or more eigenvectors coincide, so the rank of the matrix V is less than its dimensionality and determinant of the matrix V at EP must be zero. Figure 11 shows that numerically calculated hybrid quasinormal modes indeed possess this property.

Note that for the configuration with the mirror, $\det V$ is suppressed for the whole range of the values d_{gap}, indicating existence of an exceptional hypersurface [30].

[1] C. M. Bender, Making sense of non-Hermitian Hamiltonians, Rep. Prog. Phys. **70**, 947 (2007).

[2] C.-Y. Ju, A. Miranowicz, F. Minganti, C.-T. Chan, G.-Y. Chen, and F. Nori, Einstein's quantum elevator: Hermitization of non-Hermitian Hamiltonians via a generalized vielbein formalism, Phys. Rev. Res. **4**, 023070 (2022).

[3] Y. Long, H. Xue, and B. Zhang, Non-Hermitian topological systems with eigenvalues that are always real, Phys. Rev. B **105**, L100102 (2022).

[4] C. M. Bender and S. Boettcher, Real Spectra in Non-Hermitian Hamiltonians Having $\mathcal{PT}$ Symmetry, Phys. Rev. Lett. **80**, 5243 (1998).

[5] L. Feng, R. El-Ganainy, and L. Ge, Non-Hermitian photonics based on parity-time symmetry, Nat. Photonics **11**, 752 (2017).

[6] R. El-Ganainy, K. G. Makris, M. Khajavikhan, Z. H. Musslimani, S. Rotter, and D. N. Christodoulides, Non-Hermitian physics and $\mathcal{PT}$ symmetry, Nat. Phys. **14**, 11 (2018).

[7] S. K. Özdemir, S. Rotter, F. Nori, and L. Yang, Parity-time symmetry and exceptional points in photonics, Nat. Mater. **18**, 783 (2019).

[8] H. Wang, X. Zhang, J. Hua, D. Lei, M. Lu, and Y. Chen, Topological physics of non-Hermitian optics and photonics: A review, J. Opt. **23**, 123001 (2021).

[9] M. Parto, Y. G. N. Liu, B. Bahari, M. Khajavikhan, and D. N. Christodoulides, Non-Hermitian and topological photonics: Optics at an exceptional point, Nanophotonics **10**, 403 (2021).

[10] W. Chen, S. K. Özdemir, G. Zhao, J. Wiersig, and L. Yang, Exceptional points enhance sensing in an optical microcavity, Nature **548**, 192 (2017).

[11] H. Hodaei, A. U. Hassan, S. Wittek, H. Garcia-Gracia, R. El-Ganainy, D. N. Christodoulides, and M. Khajavikhan, Enhanced sensitivity at higher-order exceptional points, Nature **548**, 187 (2017).

[12] J. Wiersig, Review of exceptional point-based sensors, Photon. Res. **8**, 1457 (2020).

[13] R. Duggan, S. A. Mann, and A. Alù, Limitations of sensing at an exceptional point, ACS Photonics **9**, 1554 (2022).

[14] A. U. Hassan, B. Zhen, M. Soljacic, M. Khajavikhan, and D. N. Christodoulides, Dynamically Encircling Exceptional Points: Exact Evolution and Polarization State Conversion, Phys. Rev. Lett. **118**, 093002 (2017).

[15] X.-L. Zhang and C. T. Chan, Dynamically encircling exceptional points in a three-mode waveguide system, Commun. Phys. **2**, 63 (2019).

[16] Q. Liu, S. Li, B. Wang, S. Ke, C. Qin, K. Wang, W. Liu, D. Gao, P. Berini, and P. Lu, Efficient Mode Transfer on a Compact Silicon Chip by Encircling Moving Exceptional Points, Phys. Rev. Lett. **124**, 153903 (2020).

[17] X. Shu, A. Li, G. Hu, J. Wang, A. Alù, and L. Chen, Fast encirclement of an exceptional point for highly efficient and compact chiral mode converters, Nat. Commun. **13**, 2123 (2022).

[18] S. Longhi, $\mathcal{PT}$-symmetric laser absorber, Phys. Rev. A **82**, 031801(R) (2010).

[19] Y. D. Chong, L. Ge, and A. D. Stone, PT-Symmetry Breaking and Laser-Absorber Modes in Optical Scattering Systems, Phys. Rev. Lett. **106**, 093902 (2011).

[20] L. Feng, Z. J. Wong, R.-M. Ma, Y. Wang, and X. Zhang, Single-mode laser by parity-time symmetry breaking, Science **346**, 972 (2014).

[21] H. Hodaei, M.-A. Miri, M. Heinrich, D. N. Christodoulides, and M. Khajavikhan, Parity-time-symmetric microring lasers, Science **346**, 975 (2014).

[22] Z. J. Wong, Y.-L. Xu, J. Kim, K. O'Brien, Y. Wang, L. Feng, and X. Zhang, Lasing and anti-lasing in a single cavity, Nat. Photonics **10**, 796 (2016).

[23] D. V. Novitsky, CPA-laser effect and exceptional points in PT-symmetric multilayer structures, J. Opt. **21**, 085101 (2019).

[24] A. Pick, B. Zhen, O. D. Miller, C. W. Hsu, F. Hernandez, A. W. Rodriguez, M. Soljačić, and S. G. Johnson, General theory of spontaneous emission near exceptional points, Opt. Express **25**, 12325 (2017).

[25] L. Ferrier, P. Bouteyre, A. Pick, S. Cueff, N. H. M. Dang, C. Diederichs, A. Belarouci, T. Benyattou, J. Zhao, R. Su, J. Xing, Q. Xiong, and H. S. Nguyen, Unveiling the Enhancement of Spontaneous Emission at Exceptional Points, Phys. Rev. Lett. **129**, 083602 (2022).

[26] A. Akbarzadeh, M. Kafesaki, E. N. Economou, C. M. Soukoulis, and J. A. Crosse, Spontaneous-relaxation-rate suppression in cavities with PT symmetry, Phys. Rev. A **99**, 033853 (2019).

[27] Y. Hadad and N. Engheta, Possibility for inhibited spontaneous emission in electromagnetically open parity-time-symmetric guiding structures, Proc. Nat. Acad. Sci. **117**, 5576 (2020).

[28] S. Sunada, Enhanced response of non-Hermitian photonic systems near exceptional points, Phys. Rev. A **97**, 043804 (2018).

[29] M. Khanbekyan and J. Wiersig, Decay suppression of spontaneous emission of a single emitter in a high-Q cavity at exceptional points, Phys. Rev. Res. **2**, 023375 (2020).

[30] Q. Zhong, A. Hashemi, S. K. Özdemir, and R. El-Ganainy, Control of spontaneous emission dynamics in microcavities with chiral exceptional surfaces, Phys. Rev. Res. **3**, 013220 (2021).

[31] F. Morozko, A. Novitsky, and A. Karabchevsky, Modal Purcell factor in PT-symmetric waveguides, Phys. Rev. B **102**, 155303 (2020).

[32] G. A. Jones and D. S. Bradshaw, Resonance energy transfer: From fundamental theory to recent applications, Front. Phys. **7**, 100 (2019).

[33] Th. Förster, Energy migration and fluorescence, J. Biomed. Opt. **17**, 011002 (2012).

[34] Th. Förster, 10th Spiers Memorial Lecture. Transfer mechanisms of electronic excitation, Discuss. Faraday Soc. **27**, 7 (1959).

[35] L. Novotny and B. Hecht, *Principles of Nano-optics* (Cambridge University Press, Cambridge, 2006).

[36] S.-A. Biehs, V. M. Menon, and G. S. Agarwal, Long-range dipole-dipole interaction and anomalous Forster energy transfer across a hyperbolic metamaterial, Phys. Rev. B **93**, 245439 (2016).

[37] S. V. Gaponenko, *Introduction to Nanophotonics* (Cambridge University Press, Cambridge, 2010).

[38] D. V. Guzatov, S. V. Vaschenko, V. V. Stankevich, A. Ya. Lunevich, Yu. F. Glukhov, and S. V. Gaponenko, Plasmonic enhancement of molecular fluorescence near silver nanoparticles: Theory, modeling, and experiment, J. Phys. Chem. C **116**, 10723 (2012).

[39] A. Muravitskaya, A. Movsesyan, D. V. Guzatov, A.-L. Baudrion, P.-M. Adam, S. V. Gaponenko, and R. Vincent, Engineering of the photon local density of states: Strong Inhibition of spontaneous emission near the resonant and high-refractive index dielectric nano-objects, J. Phys. Chem. C **126**, 5691 (2022).

[40] S. V. Gaponenko, Effects of photon density of states on Raman scattering in mesoscopic structures, Phys. Rev. B **65**, 140303 (2002).

[41] S. V. Gaponenko, D. V. Guzatov, and N. D. Strekal, Strong selective anti-stokes raman scattering enhancement in plasmonics

using photon density of states engineering, J. Phys. Chem. C **125**, 27654 (2021).

[42] P. C. Nelson, The role of quantum decoherence in FRET, Biophys. J. **115**, 167 (2018).

[43] V. N. Pustovit and T. V. Shahbazyan, Resonance energy transfer near metal nanostructures mediated by surface plasmons, Phys. Rev. B **83**, 085427 (2011).

[44] T. U. Tumkur, J. K. Kitur, C. E. Bonner, A. N. Poddubny, E. E. Narimanov, and M. A. Noginov, Control of Förster energy transfer in the vicinity of metallic surfaces and hyperbolic metamaterials, Faraday Discuss. **178**, 395 (2015).

[45] L. Y. Hsu, W. Ding, and G. C. Schatz, Plasmon-coupled resonance energy transfer, J. Phys. Chem. Lett. **8**, 2357 (2017).

[46] J. Feist and F. J. Garcia-Vidal, Extraordinary Exciton Conductance Induced by Strong Coupling, Phys. Rev. Lett. **114**, 196402 (2015).

[47] J. Schachenmayer, C. Genes, E. Tignone, and G. Pupillo, Cavity-Enhanced Transport of Excitons, Phys. Rev. Lett. **114**, 196403 (2015).

[48] M. Du, L. A. Martínez-Martínez, R. F. Ribeiro, Z. Hu, V. M. Menon, and J. Yuen-Zhou, Theory for polariton-assisted remote energy transfer, Chem. Sci. **9**, 6659 (2018).

[49] J. Defrance and T. Weiss, On the pole expansion of electromagnetic fields, Opt. Express **28**, 32363 (2020).

[50] J. Ren, S. Franke, and S. Hughes, Quasinormal Modes, Local Density of States, and Classical Purcell Factors for Coupled Loss-Gain Resonators, Phys. Rev. X **11**, 041020 (2021).

[51] A. Bossart and R. Fleury, Non-hermitian time evolution: From static to parametric instability, Phys. Rev. A **104**, 042225 (2021).

[52] J. Moro, J. V. Burke, and M. L. Overton, On the Lidski-Vishik-Lyusternik perturbation theory for eigenvalues of matrices with arbitrary Jordan structure, SIAM J. Matrix Anal. Appl. **18**, 793 (1997).

[53] W. D. Heiss, Green's functions at exceptional points, Int. J. Theor. Phys. **54**, 3954 (2015).

[54] J. Wiersig, Response strengths of open systems at exceptional points, Phys. Rev. Res. **4**, 023121 (2022).

[55] A. Hashemi, K. Busch, D. N. Christodoulides, S. K. Özdemir, and R. El-Ganainy, Linear response theory of open systems with exceptional points, Nat. Commun. **13**, 3281 (2022).

[56] O. Di Stefano, N. Fina, S. Savasta, R. Girlanda, and M. Pieruccini, Calculation of the local optical density of states in absorbing and gain media, J. Phys.: Condens. Matter **22**, 315302 (2010).

[57] S. Franke, J. Ren, M. Richter, A. Knorr, and S. Hughes, Fermi's Golden Rule for Spontaneous Emission in Absorptive and Amplifying Media, Phys. Rev. Lett. **127**, 013602 (2021).

[58] Y. Wu, P. Zhou, T. Li, W. Wan, and Y. Zou, High-order exceptional point based optical sensor, Opt. Express **29**, 6080 (2021).

[59] Q. Zhong, J. Kou, S. K. Özdemir, and R. El-Ganainy, Hierarchical Construction of Higher-Order Exceptional Points, Phys. Rev. Lett. **125**, 203602 (2020).

[60] Q. Zhong, J. Ren, M. Khajavikhan, D. N. Christodoulides, S. K. Özdemir, and R. El-Ganainy, Sensing with Exceptional Surfaces in Order to Combine Sensitivity with Robustness, Phys. Rev. Lett. **122**, 153902 (2019).

[61] JCMsuite: The simulation suite for nanooptics. https://jcmwave.com, 2022.

[62] V. Lidskii, Perturbation theory of non-conjugate operators, USSR Comput. Math. Math. Phys. **6**, 73 (1966).

[63] Y. Ma and A. Edelman, Nongeneric eigenvalue perturbations of Jordan blocks, Linear Algebra Appl. **273**, 45 (1998).